Analyst

ROYAL SOCIETY OF CHEMISTRY

PAPER

View Article Online
View Journal | View Issue

Cite this: *Analyst*, 2020, **145**, 4164

In situ amplified photothermal immunoassay for neuron-specific enolase with enhanced sensitivity using Prussian blue nanoparticle-loaded liposomes

Li-Juan Zhi,[a,b] Ai-Li Sun *[a] and Dianping Tang *[b]

Methods based on prussian blue nanoparticles (PBNPs) have been reported for photothermal immunoassays in analytical nanoscience fields but most suffer from low sensitivity and are not beneficial for routine use. Herein, we design an *in situ* amplified near-infrared (NIR) photothermal immunoassay for the quantitative screening of neuron-specific enolase (NSE) on a portable thermometer using PBNP-encapsulated nanoliposomes as photosensitive materials. Biotinylated liposomes loaded with numerous prussian blue nanoparticles were synthesized through a typical reverse-phase evaporation method. The photothermal immunoassay was carried out in an anti-NSE capture antibody-coated microplate using the biotinylated anti-NSE secondary antibody. With the sandwiched immunoreaction and the biotin–avidin linkage, the subsequent photothermal measurement of PBNPs released from the liposomes with buffered surfactant including Tween 20 was conducted on a digital thermometer under near-infrared 808 nm laser irradiation, accompanied by the convertion of NIR-light wavelength to heat. Under the optimum conditions, the photothermal immunoassay displayed a wide dynamic concentration range of 0.1–100 ng mL^{-1} with a low detection limit for NSE of 0.053 ng mL^{-1}. Good reproducibility (RSD ≤ 2.78% for intra-assay; RSD ≤ 4.39% for inter-assay), high selectivity against other biomarkers, and a long-term stability (≥94.9% of the initial signal during six-month storage) were acquired in the photothermal immunoassay. Impressively, the analysis of 7 human serum specimens for target NES *via* the photothermal immunoassay also gave well-matched results with the referenced human NSE enzyme-linked immunosorbent assay.

Received 28th February 2020,
Accepted 16th April 2020

DOI: 10.1039/d0an00417k

rsc.li/analyst

Introduction

Neuron-specific enolase (NSE; known as gamma-enolase and Enolase 2), a cytoplasmic phosphopyruvate hydratase with a 46 kDa member of the Enolase family of enzymes, is the most abundant form of the glycolytic enolase found in adult neurons and is thought to serve as a growth factor in neurons.[1] It is expressed in developing neurons and glia, is known to catalyse the generation of phosphoenolpyrucate, and is suggested to possess neurotrophic activity towards neurons, likely *via* an extracellular mechanism.[2] NSE is useful in studying neuronal differentiation and is, therefore, a valuable tool for visualizing the neuronal cells and normal or malignant cells with neuroendocrine origin. The serum levels of NSE have been associated with disease such as Alzheimer's, Huntington's Chorea, neuroblastoma, head trauma, neuroendocrine malignancies, and small cell carcinomas of the lung.[3] Therefore, the sensitive and specific determination of NSE in complex systems is very important for clinical diagnostics.

Methods based on specific antigen–antibody reaction have been widely utilized for monitoring disease-related biomarkers and proteins.[4] The assays are usually implemented and executed on the basis of different signal-generation principles, *e.g.*, electrochemistry, (electro)chemiluminescence (ECL), fluorescence, mass spectroscopy, surface plasmon resonance (SPR), quartz crystal microbalance (QCM), and colorimetric protocols.[5] Despite the advances in this field, there is still a high demand to explore simple, sensitive, and portable strategies for the determination of biomolecules. The photothermal immunoassay based on the photothermal effect induced by the localized surface plasmon resonance (LSPR) of plasmonic nanoparticles has attracted increasing interest thanks to its relative simplicity and easy operation with the conversion of light wavelength to heat under irradiation.[6] Li's group, for the first time, investigated nanoparticle-mediated photothermal

[a]*Department of Chemistry and Chemical Engineering, Xinxiang University, Xinxiang 453000, China. E-mail: sunaili77@yeah.net*
[b]*Key Laboratory of Analytical Science for Food Safety and Biology (MOE & Fujian Province), Department of Chemistry, Fuzhou University, Fuzhou 350108, China. E-mail: dianping.tang@fzu.edu.cn*

effect relative to the TMB-H_2O_2 colorimetric system for the development of a visual quantitative photothermal immunoassay.[7] Liu *et al.* discovered that the photothermal nanoparticles could be applied for biosensing and immunoassay with temperature as the readout *via* enzyme-triggered crystal growth on gold nanostars.[8] Because of the unique advantages of the photothermal nanostructures, our motivation in this work is to design an advanced nanoparticle-mediated photothermal immunoassay for the sensitive detection of biomarkers.

For the successful development of photothermal immunoassays, amplification of the detectable signal is crucial in order to acquire low limits of detection and quantification.[9] A key issue is to search for high-efficiency photothermal conversion materials.[10] Recently, our group developed a near-infrared (NIR) light-based photothermal immunoassay for the qualitative or quantitative detection of prostate-specific antigen by using titanium carbide (Ti_3C_2) MXene quantum dot-loaded liposomes with an imaging camera on a smartphone.[11] However, we later found that Ti_3C_2 MXene quantum dots had a relatively low photothermal conversion efficiency. Undoubtedly, the detectable signal could be improved by coupling with other signal-amplification strategies, for *e.g.*, using self-powered temperature sensor with the Seebeck effect for photothermal–thermoelectric coupled immunoassay.[12] Unfavourably, the fabrication of photothermal–thermoelectric immunoassay by the coupled immunosensing system was relatively complicated. In contrast with Ti_3C_2 MXene, Prussian blue nanoparticles (PBNPs) are advanced and cost-effective photothermal conversion materials.[13] Fu *et al.* verified that PBNPs are near-infrared laser-driven photothermal ablation agents that are alternatives to traditional agents thanks to their good photothermal efficiency, high photothermal stability, and low cost.[14] Inspiringly, the photothermal conversion efficiency can be further enhanced by coupling with other carriers.[15]

Typically, liposomes with a highly versatile lipid bilayer structure can form enclosed vesicles with high carrying capacity to encapsulate different signal tags (*e.g.*, enzymes, quantum dots, and nanoparticles).[16] Herein, we report the proof-of-concept of a simple and powerful NIR photothermal immunoassay for the sensitive monitoring of NSE in the microplate by using Prussian blue nanoparticle-encapsulated liposomes as the photothermal conversion tags on a portable digital thermometer (Scheme 1). After the formation of sandwiched complexes, the introduction of the surfactant (Tween 20) causes the dissociation of the liposomes, releasing the encapsulated PBNPs. Under 808 nm NIR laser irradiation, the as-released PBNPs convert NIR-light wavelength to heat, thereby resulting in an increase in the temperature of the solution under study. The detectable temperature on the thermometer indirectly depends on the concentration of the target NSE in the sample. To this end, the objective of this study is to devise an *in situ* amplified and nanoparticle-mediated photothermal immunoassay for enzyme-free and cost-effective analysis of low-abundance biomarkers.

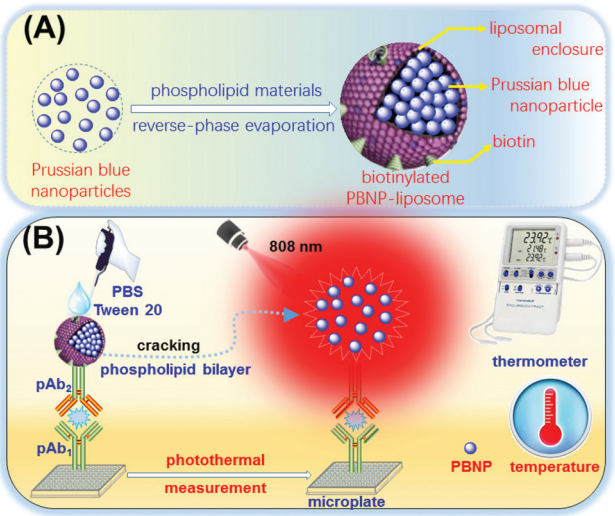

Scheme 1 Schematic illustration of the photothermal immunoassay for neuron-specific enolase (NSE): (A) architectural diagram of the biotinylated liposomes encapsulated with Prussian blue nanoparticles (PBNPs) and (B) photothermal measurement on the anti-NSE primary antibody-coated plate with a sandwiched immunoreaction format using biotinylated PBNP-liposomes as the photothermal conversion material on a portable digital thermometer under 808 nm near-infrared laser irradiation.

Experimental section

Materials and chemicals

Human neuron-specific enolase ELISA kit including various standards (sandwich, quantitative, 312.5 pg mL^{-1}–20 ng mL^{-1}, 1 × 96 tests, cat#: ab217778) was purchased from Abcam (Shanghai, China). Human neuron-specific enolase (NSE) standards (recombinant, expressed in *E. coli*) (liquid, 100 μg, cat#: SRP6108), polyclonal anti-NSE primary antibody (pAb_1; 500 μL, immunohistochemistry: 1 : 50–1 : 100, cat#: AB9698), polyclonal anti-NSE detection antibody produced in rabbit (pAb_2; 100 μg, buffered aqueous solution, isolated antibody, cat#: SAB4500768), (+)-biotin *N*-hydroxysuccinimide ester (NHS-Biotin; ≥98%, powder, cat#: H1759), bovine serum albumin (BSA; Vetc™ reagent grade, lyophilized powder, ≥98%), and streptavidin lyophilized powder from *Streptomyces avdidinii* (5.0 mg, cat# S0677) were obtained from Sigma-Aldrich (Merck KGaA, Damstadt, Germany). 1,2-Distearoyl-*sn*-glycero-3-phosphoethanolamine-*N*-biotinyl[poly(ethylene glycol)]-2000 and hydrogenated soybean phospholipids, cholesterol were obtained from Avanti Polar Lipids Inc. (Alabama, USA). Pierce™ 20× PBS Tween 20 buffer was diluted 20-fold with pure water to yield 10 mM sodium phosphate containing 0.15 M NaCl and 0.05% Tween-20, with pH of 7.4. All the high-binding polystyrene 96-well microplates were achieved from Greiner Inc. (ref. 655061, Frickenhausen, Germany). All other chemicals were of analytical grade. Ultrapure water with 18.2 MΩ cm resistivity, obtained from a Millipore water purification system (Milli-Q, Millipore), was used throughout this work. Phosphate-buffered saline (PBS, 10 mM) solutions with

different pH values were the products of Sigma-Aldrich. The washing buffer consisted of PBS (0.1 M, pH 7.4) with 0.05% (w/v) Tween 20 added to it.

Synthesis of citrate-coated Prussian blue nanoparticles (PBNPs)

At this step, citrate-coated Prussian blue nanoparticles (PBNPs) were prepared by a simple one-step aqueous solution route according to ref. 17. Prior to synthesis, two aqueous solutions (A: 20 mL, 1.0 mM $FeCl_3$ + 0.5 mmol citric acid; B: 20 mL, 1.0 mM $K_4[Fe(CN)_6]$ + 0.5 mmol citric acid) were prepared by mixing the corresponding chemicals. Following that, solution **A** was slowly added to solution **B** under vigorous stirring at room temperature. After stirring for 2 h, 10 mL acetone was injected into the above-prepared mixture. Afterwards, the resultant product was centrifuged for 15 min at 13 000*g*. The obtained precipitate was dried at 60 °C in a drying oven for further use.

Synthesis of biotinylated liposomes loaded with PBNPs

Biotinylated liposomes encapsulated with Prussian blue nanoparticles were synthesized *via* a reverse-phase evaporation method similar to ref. 18. Initially, a reverse-phase mixture was prepared by mixing chloroform, isopropyl ether, and methanol in the volume ratio of 6 : 6 : 1. Then, a lipid mixture was obtained from the resulting mixture by simultaneously adding hydrogenated soybean phospholipids (15.9 μM), cholesterol (6.4 μM), and 1,2-distearoyl-*sn-glycero*-3-phosphor ethanolamine-*N*-biotinyl[poly(ethylene glycol)]-2000 (0.2 μM). Meanwhile, 1.0 mL of PBNP aqueous solution (50 mg mL^{-1}) was added to the lipid mixture (10 mL). After shaking for 5 min on a shaker, the solvent was evaporated at 45 °C under nitrogen to form a gel-like suspension. Afterwards, uniform-size liposomes were obtained with a 200 nm polycarbonate filter on a mini-extruder (note: the excess free PBNPs could be removed during the biotin–avidin linkage). Finally, biotinylated liposomes loaded with PBNPs (designated as PBNP-liposomes) were dispersed in PBS (2.0 mL, pH 7.4) and stored at 4 °C until use.

Preparation of biotinylated anti-NSE detection antibody (Bio-pAb_2)

Biotinylated anti-NSE antibodies were prepared on the basis of the reaction between (+)-biotin *N*-hydroxysuccinimide ester (Biotin-NHS) and the antibody through a typical carbodiimide coupling.[19] Initially, 1.0 mL of 1.0 mg mL^{-1} polyclonal anti-NSE detection antibody produced in rabbit (pAb_2; buffered aqueous solution) was added into 5.0 mL of 10 mg mL^{-1} (+)-biotin *N*-hydroxysuccinimide ester solution in PBS, pH 7.4. Thereafter, the mixture was reacted for 6 h with slight shaking on a shaker at room temperature. After that, the produced precipitates during the reaction were removed by centrifugation (10 min, 5000*g*). Subsequently, biotinylated anti-NSE antibodies (Bio-pAb_2) were collected and purified by dialysis in a dialysis bag against PBS (0.1 M, pH 7.4) for 24 h at room temperature by changing the buffer every 6 h. Finally, the as-prepared Bio-pAb_2 conjugates were dispersed in PBS (1.0 mL, 0.1 M, pH 7.4) for usage.

Immunoreaction and photothermal test for target NSE

Human neuron-specific enolase standards were diluted to different concentrations with PBS (0.1 M, pH 7.4) before measurement. Firstly, polystyrene microplates (96-wells, high binding) were modified with polyclonal anti-NSE primary antibody (pAb_1; 50 μL per well, 1 : 50) in a sodium carbonate buffer (50 mM, pH 9.6) (overnight, 4 °C). Following that, the microplates were incubated with a blocking buffer (10 mM PBS + 5.0 wt% BSA, pH 7.4) for 60 min at room temperature after washing three times with the washing buffer. The microplates were washed as before. Thereafter, 50 μL of the NSE standard and 50 μL of the above-prepared Bio-pAb_2 were injected in the well and incubated for 45 min at room temperature. After another washing cycle, 100 μL of streptavidin in the blocking buffer (2.0 μg mL^{-1}) was put in the wells and reacted for 30 min under the same experimental conditions. Subsequently, the microplates were washed with washing buffer (twice) and PBS (0.1 M, pH 7.4; three times) alternatively to remove any Tween 20 remaining in the wells. After that, the resultant microplate was reacted with 50 μL of the as-prepared biotinylated liposomes loaded with PBNPs for another 25 min at room temperature. The unconjugated liposomes or PBNPs were removed by washing with PBS (0.1 M, pH 7.4). Finally, 50 μL of the washing buffer was injected in the well to dissolve the liposomes and release the encapsulated PBNPs with Tween 20 for photothermal measurement on a portable digital thermometer under 808 nm adjustable laser irradiation (1.5 W) (note: the single plate alone was installed in a fixture, which was designed and manufactured by a 3D printer). All the temperatures referred to the average values after irradiation for 8.0 min with the standard deviations (SD) in triplicate and the results were expressed as mean value ± SD of three determinations (statistical significance was defined at $P \leq 0.05$). All the measurements were performed at room temperature (25 ± 1.0 °C).

All the experiments used in this study were performed according to the Guidelines of Xinxiang University and approved by the Ethics Committee at Xinxiang University, China. Informed consent with human subjects was obtained for any experimentation.

Results and discussion

In this work, the target NSE is quantitatively determined on polyclonal anti-NSE primary antibody-coated microtiter plates by using Prussian blue nanoparticle-encapsulated nanoliposomes as the photothermal conversion materials with a digital thermometer readout (Scheme 1). Prussian blue nanoparticles exhibit highly localized surface plasmon resonance effect and high photothermal conversion efficiency under the near-infrared irradiation. The introduction of liposomes with high loading capacity is expected to enhance the sensitivity of the

photothermal immunoassay. Numerous Prussian blue nanoparticles are loaded into the biotinylated liposomes through a reverse-phase evaporation method, whereas the biotinylated antibody is prepared on the basis of a carbodiimide coupling. In the presence of target NSE, the analyte is sandwiched between the captured pAb_1 antibody and the bio-pAb_2. Using the biotin–avidin linkage, the prepared liposomes are conjugated on the plates. On the introduction of the washing buffer, the present buffered surfactant (Tween 20) dissolves the liposomes to release numerous PBNPs, thus causing an increase in the temperature of the solution under study. By monitoring the change in the temperature, the level of target NSE in the sample can be exactly evaluated *via* a fitted regression curve.

Characterization of Prussian blue nanoparticle-loaded liposomes

To achieve high photothermal conversion efficiency, the successful preparation of Prussian blue nanoparticle-encapsulated liposomes is very crucial during the synthesis. Firstly, we used a transmission electron microscope (TEM; H-7650, Hitachi Instruments Inc., Japan) to characterize the nanostructures. Fig. 1A shows the typical TEM image of the as-prepared PBNPs with a similar cuboidal morphology and the average diameter of the nanoparticles was ~12 nm. However, the size was slightly smaller than that obtained from dynamic light scattering (DLS; Zetasizer Nano S90, Malvern, UK) (16.3 ± 1.1 nm; Fig. 1A, inset), which was ascribed to the fact that the DLS data originated from the hydration radius of the nanoparticles. Also, we observed that the zeta potential of the PBNPs exhibited an intrinsic negative charge ($\xi \approx -15.7$ mV) due to the hydroxyl groups on the surface. After the formation of PBNP-encapsulated liposomes, however, almost all nanoparticles were encapsulated into the liposomes (Fig. 1B). Specifically, the average sizes increased to 120 nm in diameter, as observed from SEM (Fig. 1B), and 145 ± 17.8 nm, as observed from DLS data (Fig. 1B, inset). Such a large-sized liposome could provide more room for the encapsulation of PBNPs. Theoretically, we might roughly estimate that one 120 nm-liposome could simultaneously accommodate ~1000 PBNPs with 12 nm diameter at most (note: the calculation is based on the assumption of the volume of one spherical liposome divided by the volume of one spherical PBNP according to the equation, $V = 4/3\pi r^3$, where r stands for the corresponding radius). Moreover, the zeta potential became more negative ($\xi \approx -43.9$ mV) in comparison with that of the Prussian blue nanoparticles alone, which is ascribed to the negatively charged phosphate backbone. These results revealed that Prussian blue nanoparticles were successfully encapsulated in the liposomes.

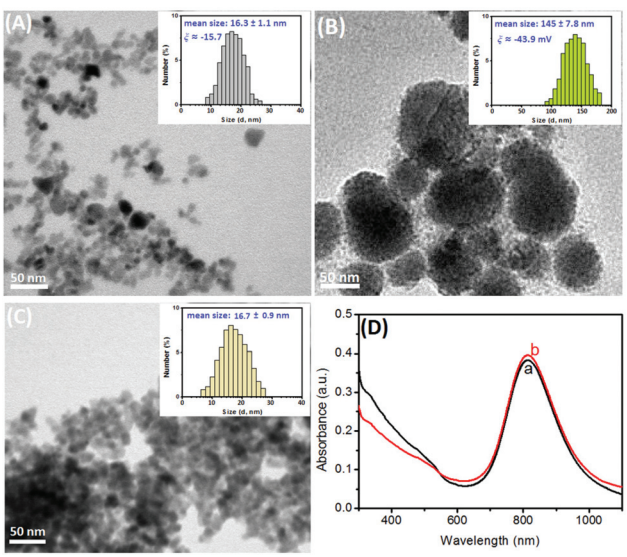

Fig. 1 Typical TEM images of (A) Prussian blue nanoparticles (inset: DLS data including size distribution and zeta potential), (B) PBNP-liposomes (inset: DLS data including size distribution and zeta potential), and (C) PBNP-liposomes (inset: DLS data); (D) Vis-NIR spectra of (a) Prussian blue nanoparticles and (b) PBNP-liposomes + Tween 20.

Logically, one question arises that whether the addition of the washing buffer (0.1 M PBS + 0.05% w/v Tween 20, pH 7.4) could readily break the liposomes and release the as-encapsulated PBNPs. As shown in Fig. 1C, the addition of the washing buffer caused the dissociation of the liposomes. A large number of Prussian blue nanoparticles were dispersed in the solution. Moreover, the average size of the released PBNPs was 16.7 ± 0.9 nm, as observed from DLS data (Fig. 1C, inset), which was almost the same as that of the newly prepared PBNPs (Fig. 1A). To further investigate the photothermal conversion characteristics of the as-released PBNPs, we utilized Vis-NIR spectroscopy to monitor the situation before (curve '*a*') and after (curve '*b*') the release of the encapsulated PBNPs from the liposomes (Fig. 1D). Obviously, the PBNP suspension had a similar absorption band between 500 nm and 1100 nm, and the maximum absorption band was ~810 nm, which was most likely due to the energy sequence of the metal-to-metal charge transfer between Fe^{II} and Fe^{III} through the cyanide bridge and which confers photothermal capabilities to the nanoparticles (upon NIR-light laser irradiation).[20] Therefore, the 'original' PBNPs before and after the release had almost no changes, and the synthesized liposomes encapsulated with Prussian blue nanoparticles could be used as photothermal conversion materials under NIR-light irradiation.

Photothermal characteristics of PBNP-loaded liposomes

Typically, Prussian blue nanoparticles have photothermal properties under NIR-light irradiation. Curve '*a*' in Fig. 2A shows the temperature changes in the as-synthesized PBNPs (50 μL, 10 mg mL^{-1} used as an example) with increasing irradiation time in PBS (0.1 M, pH 7.4). An obvious photothermal conversion behaviour for the PBNP solution alone was observed during the irradiation. As seen from curve '*b*' in Fig. 2A, the as-prepared PBNP-liposomes also exhibited a similar photothermal effect with PBNPs under the same conditions. However, it takes a relatively longer time for PBNP-liposomes to reach the steady-state temperature (curve '*b*' *vs.* curve '*a*'). The reason

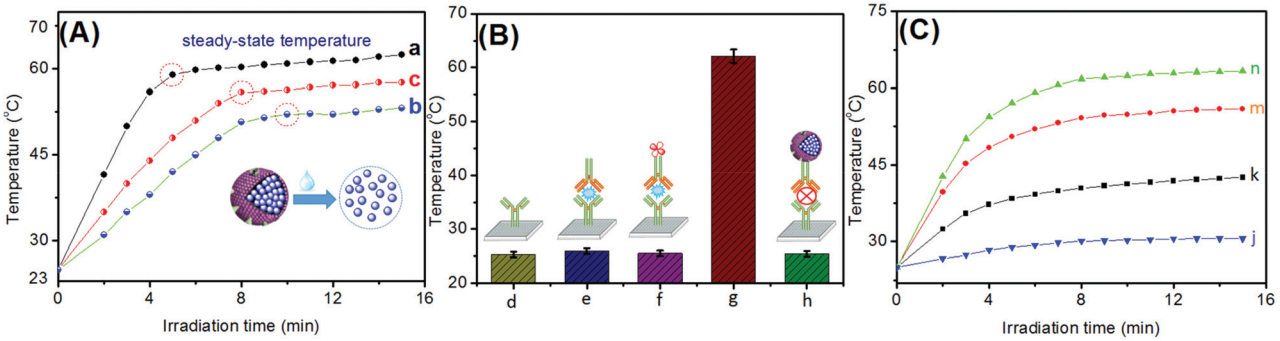

Fig. 2 (A) Temperature shifts (*vs.* irradiation time) of (a) 50-μL 10 mg mL PBNPs + 0.1 M pH 7.4 PBS, (b) 50-μL 10 mg mL PBNP-liposomes + 0.1 M pH 7.4 PBS and (c) 50-μL 10 mg mL PBNP-liposomes + 0.1 M pH 7.4 PBS + Tween 20; (B) temperatures of (d) pAb_1-coated plate, (e) Bio-pAb_2 + NSE + pAb_1, (f) avidin + Bio-pAb_2 + NSE + pAb_1, (g) PBNP-liposomes + avidin + Bio-pAb_2 + NSE + pAb_1 and (h) PBNP-liposomes + avidin + Bio-pAb_2 + pAb_1 (10 ng mL^{-1} NSE used in this cases); and (C) temperature shifts (*vs.* irradiation time) of photothermal immunoassay by using different signal-generated tags: (j) Ti_3C_2 QD-pAb_2, (k) PBNP-pAb_2, (m) Ti_3C_2 QDs-liposome-pAb_2 and (n) PBNP-liposome-pAb_2 (conditions: 1.5 V; 808 nm laser irradiation; 10 ng mL^{-1} NSE used as an example).

might be attributed to the fact that the phospholipid bilayer hindered the light adsorption to some extent. To further clarify why the liposomes are destroyed during the photothermal measurement, we collected the steady-state temperatures before and after the dissociation of PBNP-liposomes by using the buffered surfactant. Impressively, the as-released PBNPs from the PBNP-liposomes could exhibit a higher steady-state temperature than that of the PBNP-liposomes (Fig. 2A, curve '*c*'). Moreover, the temperature tended to level off more rapidly for the broken PBNP-liposomes. Therefore, the introduction of PBNP-liposomes, with the dissociation of liposomes, could be employed as signal-generation tags for photothermal measurement.

Following this, we investigated the feasibility of the photothermal immunoassay on anti-NSE pAb_1 primary antibody-coated microplate by using the biotinylated PBNP-liposomes for the detection of target NSE (10 ng mL^{-1} used as an example) after each step. Note that all the measurements were carried out in 50 μL of washing buffer (Fig. 2B). Obviously, almost no changes in the temperature relative to the background were observed at the pAb_1-coated plate (column '*d*'), Bio-pAb_2/NSE/pAb_1 (column '*e*'), and avidin/Bio-pAb_2/NSE/pAb_1 (column '*f*'), indicating that these biomolecules had no the photothermal conversion efficiency under NIR-light irradiation. Significantly, an increasing temperature change appeared upon the introduction of PBNP-liposomes (column '*g*'). The increased temperature derived from the PBNPs towards the conversion of NIR-light adsorption to heat. Certainly, a puzzling question is whether PBNP-liposomes could be non-specifically adsorbed on the microplate. To verify this issue, pAb_1-coated microplate interacted with Bio-pAb_2, streptavidin, and PBNP-liposomes in sequence without the target NSE. As indicated from column '*h*', the steady-state temperature was almost the same as the background. The results also suggested that our system could be preliminarily applied for NSE detection on a thermometer.

To further elucidate the *in situ* amplified capacity of PBNP-liposomes for photothermal immunoassays relative to our previous work (Ti_3C_2 MXene quantum dots-encapsulated liposomes)[11] and PBNPs alone, the same-concentration NSE standards (10 ng mL^{-1} used in this case) were determined on a pAb_1-coated microplate by using Ti_3C_2 QD-pAb_2, PBNP-liposomes, PBNP-pAb_2, and Ti_3C_2 QDs-liposomes (note: PBNP-pAb_2, Ti_3C_2 QD-pAb_2, and Ti_3C_2 QDs-liposomes were prepared by referring to ref. 21 and 11, respectively). The assays were carried out by adopting the same protocols. The experimental results for the temperature changes *versus* irradiation times are given in Fig. 2C. Evidently, the use of Ti_3C_2 QD-pAb_2 (curve '*j*') and PBNP-pAb_2 (curve '*k*') exhibited low shifts in the temperature. In contrast, the introduction of same-sized liposomes for Ti_3C_2 QDs-liposomes (curve '*m*') and PBNP-liposomes (curve '*n*') caused greater changes in the temperature than those of the corresponding Ti_3C_2 QD-pAb_2 (curve '*j*') and PBNP-pAb_2 (curve '*k*'). It is easy to understand that the liposomes could provide a large room for the loading of PBNPs and Ti_3C_2 QDs. The results indicated that the high loading amount of the same kind of nanoparticles could amplify the detectable signal to some extent. Moreover, the large-sized PBNPs alone for PBNP-pAb_2 (curve '*k*') displayed a higher change in the temperature than that of the small-sized Ti_3C_2 QDs alone (curve '*j*') because the encapsulated nanoparticles in the liposomes had different sizes (~12 nm for PBNPs *vs.* ~3.4 nm for Ti_3C_2 QDs[11]) in these two systems. Theoretically, the encapsulated amount of Ti_3C_2 QDs was more than that of PBNPs in the same-sized liposomes. However, the shift in the temperature due to use of Ti_3C_2 QDs-liposomes (curve '*m*') was less than that for when PBNP-liposomes (curve '*n*') was used. The reason was attributed to the fact that they had different photothermal conversion efficiencies (η). To this end, the *in situ* amplified capacity on using PBNP-liposomes as the photothermal material was further demonstrated by calculating the photothermal conversion efficiency. All the photothermal conversion efficien-

cies were obtained from the plates under 808 nm NIR-light irradiation at 1.5 W for 1.0 mg mL^{-1} samples. The detailed calculation method has been described in our previous report.[11] The photothermal conversion efficiencies (η) were evaluated using the following equation:[22]

$$\eta_T = [hA\ (T_{max} - T_{surr}) - Q_0]/I(1 - 10^{-A808})$$

where h is for the heat transfer coefficient, A is the surface area of heat transfer of this system, T_{max} is the maximum temperature, T_{surr} is the surrounding temperature, Q_0 is the rate of heat input due to absorption of light energy by water, I is the laser power, and A_λ is the absorbance of the sample at 808 nm. The experimental results indicated that the photothermal conversion efficiencies (η) were 17.8% for Prussian blue nanoparticles (PBNPs), 36.7% for PBNP-liposomes, and 31.4% for Ti_3C_2 MXene quantum dots-loaded liposomes. Therefore, the PBNP-liposomes could be used to improve the sensitivity of the photothermal immunoassay, which was mainly ascribed to the high photothermal conversion efficiency. In addition, all the steady-state temperatures in the cases reached equilibrium after irradiation for 8.0 min. To avoid possible errors resulting from different NSE standards or samples, all the temperatures on the thermometer were collected and registered as the immunosensing signal after 8.0 min of irradiation.

Optimization of experimental conditions

In this system, the photothermal immunoassay mainly consisted of the immunoreaction, the biotin–avidin linkage, and liposome dissociation. Generally, the liposomes are easily broken by a buffered surfactant. In this regard, we initially investigated the effect of immunoreaction time on the analytical performance of the photothermal immunoassay. As shown in Fig. 3A, the steady-state maximum temperatures were reached after 45 min. As is well-known, the ratio of immunoreaction between the antibody and antigen usually increases with increasing times and then reaches equilibrium. In the same way, a similar phenomenon could also be found for the biotin–avidin linkage (Fig. 3B). To ensure adequate reaction and shorten the assay time, 45 min and 25 min were used for the antigen–antibody reaction and the biotin–avidin linkage, respectively.

Dose responses of the photothermal immunoassay for target NSE

Using the biotinylated PBNP-liposomes as the signal-generated tags, target NSE standards with different concentrations were determined on pAb_1-coated microplates with biotinylated pAb_2 by a sandwiching reaction accompanying the biotin–avidin linkage. Temperatures were recorded using a portable digital thermometer in 50 μL of the washing buffer after 8.0 min of NIR-light irradiation with 808 nm wavelength at 1.5 W cm^{-2} power density. To compensate the temperature variation caused by the surrounding ambient temperature and the as-prepared signal tags in a different facility, the temperature change (%) relative to the background was used for linear fitting by the following equation: $(T_{max} - T_{surr})/T_{surr} \times 100\%$, where T_{max} and T_{surr} stand for the measurable steady-state temperature and the surrounding temperature, respectively. Fig. 4A shows the temperature change of the photothermal immunoassay towards NSE standards with various concentrations. It was found that the temperature changes were not obvious when the concentration of NSE was ≤0.1 ng mL^{-1} or ≥100 ng mL^{-1}, and the whole temperature changes exhibit an *S*-shaped relationship within the dynamic range from 0.01 ng mL^{-1} and 1000 ng mL^{-1} of NSE. A good linear relationship between the temperature change (%) and the decimal logarithm of the NSE levels could be obtained in the range from 0.01 ng mL^{-1} to 30 ng mL^{-1} with a limit of detection (LOD) of 0.053 ng mL^{-1} (S/N = 3). The linear regression equation was y (%) = (77.45 ± 4.27) + (70.71 ± 3.84) × log $C_{[NSE]}$ (ng mL^{-1}; r = 0.9927, n = 7). Significantly, the comparable analytical properties could also be obtained relative to other NSE detection schemes including the assay method, linear range, and LOD (Table 1). Although the LOD of the photothermal immunoassay was higher than those of partial electrochemical or fluorescence immunoassays, our developed strategy did not need expensive instrumentation. Further, the LOD of our system was acceptable in comparison with the commercialized NSE ELISA kits from different companies (*e.g.*, 0.023 ng mL^{-1} for Abcam cat# ab217778; 1.875 ng mL^{-1} for FineTest cat# ESH0022; 0.038 ng mL^{-1} for R&D System cat# DENL20; 0.0508 ng mL^{-1} for Abcam cat# ab233626).

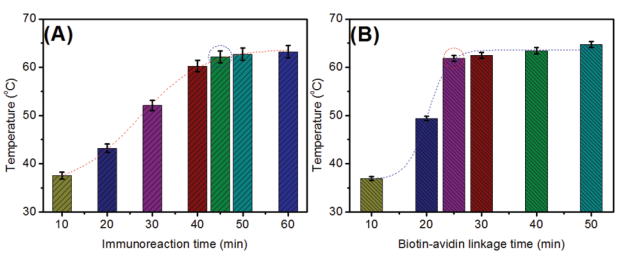

Fig. 3 Dependence of temperature on (A) immunoreaction time and (B) the biotin–avidin linkage time of the photothermal immunoassay (10 ng mL^{-1} NSE used in these cases).

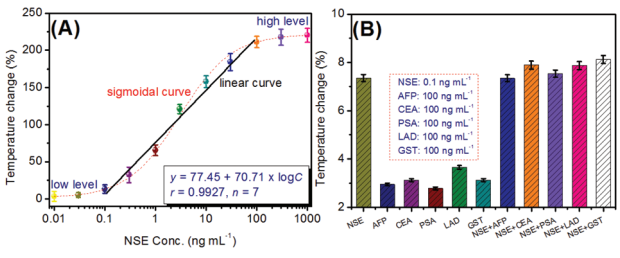

Fig. 4 (A) Calibration plots of the photothermal immunoassay towards NSE levels by using PBNP-liposomes as the signal-generation tags at 1.5 V under 808 nm NIR-light irradiation and (B) the specificity of photothermal immunoassay against NSE, AFP, CEA, PSA, LAD, and GST.

Table 1 Comparative study of PBNP-liposome-based photothermal immunoassay with other NSE detection strategies

Detection method[a]	Linear range ng mL^{-1}	LOD ng mL^{-1}	Ref.
ECL immunoassay	5.5×10^{-7}–5.5	1.8×10^{-7}	23
EC immunoassay	1.0×10^{-4}–100	52.14×10^{-6}	24
PEC immunosensor	75–723	0.12	25
EC immunoassay	1.0–1000	0.3	26
CL immunoassay	0.05–64	0.044	27
SERS assay	—[b]	0.74	28
FL immunoassay	—	0.5	29
SERS lateral flow strip	1.0–75	0.86	30
EC immunoassay	0.1–2000	0.05	31
ICA measurement	—	0.0426	32
LC-MS/MS	5.0–500	0.038	33
Photothermal assay	0.1–100	0.053 ng mL^{-1}	This work

[a] ECL: electrochemiluminescence; EC: Electrochemical; PEC: photoelectrochemical; SERS: surface-enhanced Raman scattering; FL: fluorescent; CL: chemiluminescence; ICA: immunochromatograhic assay. [b] No detected.

Reproducibility, selectivity, and storage stability

Although the formed immunocomplex *via* specific antigen–antibody reaction might be broken under drastic conditions (*e.g.*, alkalinic or acidic solutions or chaotropic agents), interestingly, the biomolecules usually suffer from serious functional damage or may even be detached from the plates. So, the as-prepared immunosensing interface was disposable (*i.e.*, one well per sample) in this work. In this regard, the reproducibility of the photothermal immunoassay was evaluated for the detection of target NES using the pAb_1-coated microplates, Bio-pAb_2 and PBNP-liposomes with same or different-preparation batches. As shown in Table 2, the relative standard deviations (RSDs) were less than 2.78% for intra-assay and 4.39% for inter-assay in triplicate towards low/middle/high-concentration target analysts. So, the reproducibility of the photothermal immunoassay is acceptable.

As a newly developed method for clinical diagnostic, the selectivity of this system is very important because different proteins or cancer biomarkers may be present in serum samples. To demonstrate this, we selected several biomarkers (as examples) including alpha-fetoprotein (AFP), carcinoembryonic antigen (CEA), prostate-specific antigen (PSA), lactate acid dehydrogenase (LAD), and glutathione-S-transferase (GST) to monitor the specificity of this method. As seen from Fig. 4B, these non-target analytes including AFP, CEA, PSA, LAD, and GST alone or mixed with the NSE did not interfere with the significant temperature change of the photothermal immunoassay and all the temperature changes (% *vs.* the corresponding control tests) were below 3.0% (*i.e.*, by subtracting the corresponding control tests), thus indicating good specificity and selectivity towards the target NSE.

Further, the storage stability of pAb_1-coated microplates, Bio-pAb_2, and PBNP-liposomes was investigated for a 6-month period by storing them at 4 °C when not in use. During this period, they were used for the detection of target NSE (10 ng mL^{-1} used as an example) intermittently. The experimental results indicated that the temperature changes (%) were 146.2%, 143.4%, 140.8%, 138.9%, 137.6%, and 135.8% in the 1st, 2nd, 3rd, 4th, 5th, and 6th month, respectively (note: the temperature change of the newly prepared immunoassay system was 148.1%) with satisfactory storage stability.

Table 2 Reproducibility of the photothermal immunoassay

	Conc. ng mL^{-1}	Assay time; temperature (°C) 1	2	3	RSD (%)
Intra-assay	0.1	26.8	27.5	27.1	1.29
	10	63.2	61.6	62.4	1.28
	100	79.2	75.6	79.5	2.78
Inter-assay	0.1	25.6	27.9	26.4	4.38
	10	64.5	60.2	61.8	3.49
	100	73.2	79.9	76.4	4.39

Evaluation of method accuracy for human serum specimens

The accuracy of the photothermal immunoassay method was evaluated for the analysis of human serum specimens. Initially, we collected 7 serum samples from the Hospital of Xinxiang University according to the guidelines of the University (note: the NSE concentrations in the samples were simultaneously determined by using commercialized human NSE ELISA kit and executed by medical professionals in the hospital, Acknowledgment). Thereafter, these samples were measured using the photothermal immunoassays. The results obtained by the two methods are listed in Table 3. For comparison, we used two methods including a least-square regression and a *t*-test to evaluate the accuracy of this method. As indicated in Table 3, all the t_{exp} values were below t_{crit} ($t_{crit[2,0.05]}$ = 4.30). Moreover, the intercept and slope in the regression equation were close to the ideal values of "0" and

Table 3 Accuracy evaluation of the photothermal immunoassay for human serum specimens by using commercial human NSE ELISA kit as the reference

Sample no.	Method; Conc. (mean ± SD, ng mL^{-1} n = 3)[a] Photothermal immunoassay	Human NSE ELISA kit	t_{exp}
1	567.3 ± 12.3	592.1 ± 9.9	2.72
2	68.9 ± 5.1	56.2 ± 6.1	2.77
3	231.3 ± 11.2	257.2 ± 13.5	2.56
4	892.3 ± 6.4	901.1 ± 5.8	1.76
5	632.4 ± 23.4	674.3 ± 18.5	2.43
6	478.9 ± 17.9	443.8 ± 14.6	2.63
7	132.4 ± 6.5	123.1 ± 7.8	1.59

[a] NSE concentrations in the samples were calculated by referring to the dilution ratio because the normal level (threshold) of NSE in human serum is 12.5 mg L^{-1}.[34] The regression equation (linear) for the average values between two methods was fitted: $y = 1.0309x - 6.9089$ (R^2 = 0.9933, n = 7, x axis: by the photothermal immunoassay, y axis: by the human NSE ELISA kit).

"1", respectively. On the basis of these experimental results, we might ensure that almost no significant differences at the 0.05 significance level were encountered in the analysis of 7 human serum specimens between the photothermal immunoassay and the referenced ELISA kit for the determination of target NSE, suggesting good accuracy between the two methods.

To further embody the advantages of the photothermal immunoassay for the detection of target NSE in complex systems, five NSE standards including 0.5, 10, 20, 40, and 80 ng mL^{-1} were spiked into normal calf serum without the target analyte (note: the aim of using calf serum is to avoid the interference of NSE in human serum). The contents assayed by the photothermal immunoassay were 0.52, 9.56, 22.54, 36.89, and 84.56 ng mL^{-1} for the above-mentioned analytes, respectively. The recoveries were 104%, 95.6%, 112.7%, 92.2%, and 105.7%, respectively. Therefore, the developed photothermal immunoassay can be considered as an optional scheme for NSE detection in clinic diagnosis.

Conclusions

In this contribution, we successfully devise a sensitive photothermal immunoassay protocol for the simple and feasible screening of neuron-specific enolase on a portable digital thermometer by using Prussian blue nanoparticle-loaded liposomes as the photothermal conversion materials. These results from the TEM image indicated that numerous Prussian blue nanoparticles were encapsulated in the liposome, thus resulting in signal amplification during the measurement. Good reproducibility, high specificity, and long-term stability were acquired in the analysis of the target NSE. Compared to our previous work using MXene quantum dots-encapsulated liposomes[11] and pure Prussian blue nanoparticle-based strategy, PBNP-liposome-based photothermal immunoassay could exhibit a relatively high temperature response. Significantly, our strategy was cheaper (~USD $1.792 for a single test) than that of commercialized human NSE ELISA kit (~USD $10.92 for a single test, product cat# no.: ab217778 from Abcam; ~USD $12.45 for a single test, product cat# no.: MAK178 from Sigma-Aldrich), thereby opening new opportunities for protein diagnostics and biosecurity.

Conflicts of interest

There are no conflicts to declare.

Acknowledgements

This work was financially supported by the National Natural Science Foundation of China (Grant No.: 51802275), the Key Scientific and Technological Research Project of Henan Province (Grant No.: 202102310298), the Research Fund for the Technological Innovative Scholar of Xinxiang University (China), and the Henan Photoelectrocatalytic Material and Micro-nano Application Technology Academician Workstation, Xinxiang, Henan 450003, China.

References

1 P. Marangos, J. Polak and A. Pearse, *Trends Neurosci.*, 1982, **5**, 193–196.
2 C. Xu, Y. Luo, S. Li, Z. Li, L. Jiang, G. Zhang, L. Owusu and H. Chen, *Biosci. Rep.*, 2019, **39**, 20192732.
3 A. Haque, R. Polcyn, D. Matzelle and B. Banik, *Brain Sci.*, 2018, **8**, 33.
4 (*a*) J. Shu and D. Tang, *Anal. Chem.*, 2020, **92**, 363–377; (*b*) J. Shu and D. Tang, *Chem. – Asian J.*, 2017, **12**, 2780–2789; (*c*) X. Pei, B. Zhang, J. Tang, B. Liu, W. Lai and D. Tang, *Anal. Chim. Acta*, 2013, **758**, 1–18.
5 (*a*) Q. Zhou and D. Tang, *Trends Anal. Chem.*, 2020, **124**, 115814; (*b*) S. Lv, K. Zhang, L. Zhu and D. Tang, *Anal. Chem.*, 2020, **92**, 1470–1476; (*c*) R. Ren, G. Cai, Z. Yu, Y. Zeng and D. Tang, *Anal. Chem.*, 2018, **90**, 11099–11105; (*d*) Z. Qiu, J. Shu and D. Tang, *Anal. Chem.*, 2017, **89**, 5152–5160; (*e*) S. Jeong, M. Park, W. Song and H. Kim, *Clin. Biochem.*, 2020, **78**, 43–57.
6 (*a*) J. Zhang, H. Xing and Y. Lu, *Chem. Sci.*, 2018, **9**, 3906–3910; (*b*) V. Shirshahi, S. Tabatabaei, S. Hatamie and R. Saber, *Colloids Surf., B*, 2020, **186**, 110721; (*c*) L. Lu, M. Wang, D. Zhang and H. Zhang, *Analyst*, 2019, **144**, 6647–6652; (*d*) B. Zhang, Y. Jia, J. Wang, H. Chang, Z. Zhao and Y. Cheng, *Process Biochem.*, 2019, **87**, 66–72; (*e*) G. Fu, S. Sanjay, M. Dou and X. Li, *Nanoscales*, 2016, **8**, 5422–5423; (*f*) G. Fu, Y. Zhu, K. Xu, W. Wang, R. Hou and X. Li, *Anal. Chem.*, 2019, **91**, 13290–13296.
7 G. Fu, S. Sanjay, W. Zhou, R. Brekken, R. Kirken and X. Li, *Anal. Chem.*, 2018, **90**, 5930–5937.
8 Y. Liu, M. Pan, W. Wang, Q. Jiang, F. Wang, D. Pang and X. Liu, *Anal. Chem.*, 2019, **91**, 2086–2092.
9 (*a*) H. Ren, Q. Han, S. Zhang, Y. Huang, Y. Chen, H. Dai, J. Yan and Y. Lin, *Sens. Actuators, B*, 2020, **309**, 127823; (*b*) Z. Wei, Y. Liu, Z. Ma and H. Han, *Biosens. Bioelectron.*, 2020, **150**, 111951.
10 L. Huang, Y. Li, Y. Du, Y. Zhang, X. Wang, Y. Ding, X. Yang, F. Meng, J. Tu, L. Luo and C. Sun, *Nat. Commun.*, 2019, **10**, 4871.
11 G. Cai, Z. Yu, P. Tong and D. Tang, *Nanoscale*, 2019, **11**, 15659.
12 L. Huang, J. Chen, Z. Yu and D. Tang, *Anal. Chem.*, 2020, **92**, 2809–2814.
13 (*a*) X. Han, S. Lin, Y. Li, C. Cheng and X. Han, *Anal. Chim. Acta*, 2020, **1098**, 117–124; (*b*) H. Hoffman, L. Chakrabarti, M. Dumont, A. Sandler and R. Fernandes, *RSC Adv.*, 2014, **4**, 29729–29734.
14 G. Fu, W. Liu, S. Feng and X. Yue, *Chem. Commun.*, 2012, **48**, 11567–11569.
15 X. Li, L. Yang, C. Men, Y. Xie, J. Liu, H. Zou, Y. Li, L. Zhan and C. Huang, *Anal. Chem.*, 2019, **91**, 4444–4450.

16 (*a*) Y. Lin, Q. Zhou, Y. Zeng and D. Tang, *Microchim. Acta*, 2018, **185**, 311; (*b*) R. Ren, G. Cai, Z. Yu and D. Tang, *Sens. Actuators, B*, 2018, **265**, 174–181; (*c*) Y. Lin, Q. Zhou and D. Tang, *Anal. Chem.*, 2017, **89**, 11803–11810.
17 (*a*) M. Shokouhimehr, E. Soehnlen, A. Khitrin, S. Basu and S. Huang, *Inorg. Chem. Commun.*, 2010, **13**, 58–61; (*b*) B. Zhang, H. Ding, Q. Chen, T. Wang and K. Zhang, *Analyst*, 2019, **144**, 4858–4864.
18 (*a*) M. Bui, S. Ahmed and A. Abbas, *Nano Lett.*, 2015, **15**, 6239–6246; (*b*) J. Tang, Y. Huang, H. Liu, C. Zhang and D. Tang, *Biosens. Bioelectron.*, 2016, **79**, 508–514.
19 (*a*) V. Kandimalla, V. Tripathi and H. Ju, *Biomaterials*, 2006, **27**, 1167–1174; (*b*) Y. Lin, Q. Zhou, D. Tang, R. Niessner and D. Tang, *Anal. Chem.*, 2017, **89**, 5637–5645.
20 J. Cano-Mejia, M. Bookstaver, E. Sweeney, C. Jewell and R. Fernandes, *Biomater. Sci.*, 2019, **7**, 1875–1887.
21 G. Hong, D. Zhang, Y. He, Y. Yang, P. Chen, H. Yang, Z. Zhou, Y. Liu and Y. Wang, *Anal. Bioanal. Chem.*, 2019, **411**, 6837–6845.
22 D. Roper, W. Ahn and M. Hoepfner, *J. Phys. Chem. C*, 2007, **111**, 3636–3641.
23 X. Zheng, G. Mo, Y. He, D. Qin, X. Jiang, W. Mo and B. Deng, *Microchim. Acta*, 2019, **186**, 817.
24 C. Zhang and Z. Ma, *Biosens. Bioelectron.*, 2019, **143**, 111612.
25 R. Soomro, N. Kalwar, A. Avci, E. Pehlivan, K. Hallam and M. Willander, *Biosens. Bioelectron.*, 2019, **141**, 11131.
26 J. Amani, M. Maleki, A. Khoshroo, A. Sobhani-Nasab and R. Rahimi-Nasrabadi, *Anal. Biochem.*, 2018, **548**, 53–59.
27 Y. Mao, N. Wang, F. Yu, S. Yu, L. Liu, Y. Tian, J. Wang, Y. Wang, L. He and Y. Wu, *Analysts*, 2019, **144**, 4813–4819.
28 D. Li, M. Yang, H. Li, L. Mao, Y. Wang and B. Sun, *New J. Chem.*, 2019, **43**, 5925–5931.
29 M. Toma, S. Izumi and K. Tawa, *Analyst*, 2018, **143**, 858–864.
30 X. Gao, P. Zheng, S. Kasani, S. Wu, F. Yang, S. Lewis, S. Nayeem, E. Engler-Chiurazzi, J. Wigginton, J. Simpkins and N. Wu, *Anal. Chem.*, 2017, **89**, 10104–10110.
31 B. Wang, T. Liang, J. Li, H. Yu and X. Chu, *Int. J. Electrochem. Sci.*, 2017, **12**, 7607–7615.
32 K. Xiao, K. Wang, W. Qin, Y. Hou, W. Lu, H. Xu, Y. Wo and D. Cui, *Talanta*, 2017, **164**, 463–469.
33 S. Torsetnes, S. Lovbak, C. Laus, H. Lund, M. Nordlund, E. Paus, T. Halvorsen and L. Reubsaet, *J. Chromatogr. B: Anal. Technol. Biomed. Life Sci.*, 2013, **929**, 125–132.
34 J. Wu, Z. Fu, F. Yan and H. Ju, *Trends Anal. Chem.*, 2007, **26**, 679–688.